Inorganic Chemistry

Article

pubs.acs.org/IC

Magnetic Structure and Exchange Interactions in Quasi-One-Dimensional $MnCl_2(urea)_2$

Jamie L. Manson,[*,†] Qing-zhen Huang,[‡] Craig M. Brown,[‡,§] Jeffrey W. Lynn,[‡] Matthew B. Stone,[∥] John Singleton,[⊥] and Fan Xiao[#]

[†]Department of Chemistry and Biochemistry, Eastern Washington University, Cheney, Washington 99004, United States
[‡]NISTCenter for Neutron Research, National Institute of Standards and Technology, Gaithersburg, Maryland 20899, United States
[§]Department of Chemical and Biochemical Engineering, University of Delaware, Newark, Delaware 19716, United States
[∥]Quantum Condensed Matter Division, Oak Ridge National Laboratory, Oak Ridge, Tennessee 37830, United States
[⊥]National High Magnetic Field Laboratory, Los Alamos National Laboratory, Los Alamos, New Mexico 87545, United States
[#]Center for Materials Physics, Durham University, Durham DH1 3LE, United Kingdom

Supporting Information

ABSTRACT: $MnCl_2(urea)_2$ is a new linear chain coordination polymer that exhibits slightly counter-rotated Mn_2Cl_2 rhomboids along the chain-axis. The material crystallizes in the noncentrosymmetric orthorhombic space group *Iba*2, with each Mn(II) ion equatorially surrounded by four Cl^- that lead to bibridged ribbons. Urea ligands coordinate via O atoms in the axial positions. Hydrogen bonds of the Cl···H−N and O···H−N type link the chains into a quasi-3D network. Magnetic susceptibility data reveal a broad maximum at 9 K that is consistent with short-range magnetic order. Pulsed-field magnetization measurements conducted at 0.6 K show that a fully polarized magnetic state is achieved at B_{sat} = 19.6 T with another field-induced phase transition occurring at 2.8 T. Zero-field neutron diffraction studies made on a powdered sample of $MnCl_2(urea)_2$ reveal that long-range magnetic order occurs below T_N = 3.2(1) K. Additional Bragg peaks due to antiferromagnetic (AFM) ordering can be indexed according to the *Ib′a*2′ magnetic space group and propagation vector τ = [0, 0, 0]. Rietveld profile analysis of these data revealed a Néel-type collinear ordering of Mn(II) ions with an ordered magnetic moment of 4.06(6) μ_B (5 μ_B is expected for isotropic $S = {}^5/_2$) oriented along the *b*-axis, i.e., perpendicular to the chain-axis that runs along the *c*-direction. Owing to the potential for spatial exchange anisotropy and the pitfalls in modeling bulk magnetic data, we analyzed inelastic neutron scattering data to retrieve the exchange constants: J_c = 2.22 K (intrachain), J_a = −0.10 K (interchain), and D = −0.14 K with $J > 0$ assigned to AFM coupling. This J configuration is most unusual and contrasts the more commonly observed AFM interchain coupling of 1D chains.

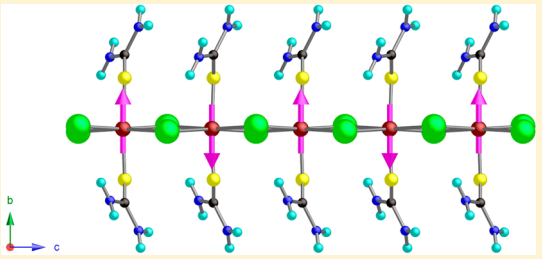

INTRODUCTION

Low-dimensional (0-, 1-, and 2D) molecular magnetic materials continue to attract much attention in our laboratory and worldwide.[1] Current interest in such materials is driven by the rich variety of magnetic ground and excited states that can be observed, especially at high magnetic fields, low temperatures, or high pressures. In order to better understand the underlying magnetism of these systems it is imperative that we understand the relationship between the lattice and spin degrees of freedom. If at all possible, neutron scattering is most useful as it can reveal phenomena not observed by macroscopic measurement techniques and, in particular, the interplay between magnetic structure and resulting spin excitations.

Metal-halide compounds often form low-dimensional crystal structures and continue to elicit much interest. For example, anhydrous $CuCl_2$ has been shown to exhibit spin-driven ferroelectricity and strong magnetoelectric coupling[2a] whereas $CuBr_2$ is a multiferroic with a relatively high T_N of 73.5 K.[2b] A variety of hydrates (e.g., $MnCl_2{\cdot}2H_2O$),[3a] doped variants (e.g., $Fe_{1-x}Ni_xCl_2{\cdot}2H_2O$),[3b] and alkali metal salts such as $CsNiCl_3$,[4a] Rb_2CrCl_4,[4b,c] and Rb_2MnCl_4[4d] also exist, with the latter three compounds being described, respectively, as a 1D Haldane chain and 2D Heisenberg square lattices. Neutron scattering played a key role in characterizing the magnetic ground states in several of these materials.[4]

The structural and magnetic diversity of metal-halides can be expanded even further by incorporation of organic Lewis bases such as pyrazine (pyz),[1b−e,5] pyrazine-*N*,*N*′-dioxide (pyzdo),[6] tetrahydrofuran (THF),[7] pyridine (py),[8] 2,2′-bipyridine (2,2′-bipy),[9] and 4,4′-bipyridine (4,4′-bipy),[10] just to list a few. Interesting physical properties presented by these materials include antiferro- (AFM), ferri- (FIM), ferro- (FM), and metamagnetism (MM), with the particular state depending on the metal ion, its oxidation number, and the presence of any spin-exchange anisotropy.[11] Binuclear[12] and chain-type[7−9]

Received: September 19, 2015

DOI: 10.1021/acs.inorgchem.5b02162
Inorg. Chem. XXXX, XXX, XXX−XXX

structural motifs that have been reported primarily consist of bibridged M−Cl_2−M cores as opposed to single M−Cl−M interactions. It seems that the organic ligand may perturb the M−Cl−M angle in both bridge types which in turn alter the sign and magnitude of the (super)exchange interaction. However, truly systematic magnetostructural studies are lacking in these high-spin Mn(II) complexes.

In our quest to design model systems composed of selected types of interchain or interlayer hydrogen bonds, we have been exploring urea [$CO(NH_2)_2$] as an ancillary ligand in conjunction with metal-halide structural units. Urea contains amine groups that could facilitate extensive hydrogen bond formation with suitable ligands such as Cl^- and Br^-. Other examples of coordination polymers that contain metal-bound urea include $Mn(HCO_2)_2(urea)_2$,[13] $[Gd(urea)_4(H_2O)_2]_2[Cr(CN)_6]_2$,[14] and $[Mn(urea)_2(H_2O)]_2[Nb(CN)_8]$.[15] In the present work, we describe the structural and magnetic properties of $MnCl_2(urea)_2$ which contains bibridged Mn−Cl_2−Mn linear chains linked in three-dimensions by Cl···H−N and O···H−N hydrogen bond types. Magnetometry and neutron scattering probes demonstrated short- and long-range (T_N = 3.1 K) magnetic ordering of the high-spin ($S = {}^5/_2$) ions with the ordered moments aligned AFM along the chain *c*-axis but weakly FM along the *a*- and *b*-directions. This unique intra- and interchain coupling scheme was not evident from bulk magnetometry data and revealed only through neutron experimentation.

EXPERIMENTAL SECTION

Synthesis. All chemicals were purchased from Aldrich Chemical Co. and used as received. In a typical synthesis, $MnCl_2·4H_2O$ (0.3503 g, 1.77 mmol) and urea (0.2126 g, 3.54 mmol) were dissolved separately in ∼10 mL of ethanol. While stirring, the ethanolic $MnCl_2$ solution was poured into the urea solution to yield a pale pink precipitate. The solid was collected by suction filtration and dried *in vacuo* for around 2 h (0.4005 g, 92% yield). Pink crystals suitable for the X-ray structure determination were obtained by slow evaporation of the filtrate over a period of a few days. The neutron sample was prepared in analogous fashion, but by scaling up the reaction accordingly to provide a 2-g batch.

X-ray Crystallography. A pink parallelepiped crystal measuring 0.25 × 0.06 × 0.06 mm^3 was mounted on a Bruker AXS SMART X-ray diffractometer equipped with a CCD area detector. Monochromated Mo Kα radiation (λ = 0.710 73 Å) was used in the data collection. Approximately a hemisphere of data was measured to a resolution of 0.75 Å at 295 K. The area detector frames were integrated by use of the program SAINT,[16] and the resulting intensities corrected for absorption by Gaussian integration (SADABS).[17] The SHELXTL[18] program package was employed in the structure solution, using direct methods and full matrix least-squares refinement on F^2 (using all data).[18] Urea H atoms were placed in idealized positions and allowed to ride on the atom to which they are attached. All non-hydrogen atoms were refined with anisotropic thermal parameters. Additional details of the data collection are given in Tables 1−3 which list selected bond lengths and angles as well as hydrogen bond parameters. Further structural details are available as electronic Supporting Information.

Magnetic Susceptibility. Quasistatic measurements were conducted using a Quantum Design PPMS-9 T ac/dc magnetometer equipped with the reciprocating sample option (RSO). Polycrystalline samples of $MnCl_2(urea)_2$ were loaded into gelatin capsules and mounted on the end of a carbon fiber rod. The samples were cooled in approximately zero-field to the lowest attainable base temperature of 2 K, and data were collected upon warming in a 0.1 T magnetic field. Experimental susceptibilities were corrected for the diamagnetism of the constituent atoms.

Table 1. Crystallographic Data for $MnCl_2(urea)_2$ Obtained from X-ray and Neutron Diffraction

	$C_2H_8N_4O_2MnCl_2$	$C_2H_8N_4O_2MnCl_2$
diff method	X-rays	neutrons
sample type	single crystal	powder
fw, g/mol	245.96	245.96
T, K	295	1.4
space group	*Iba*2	*Iba*2
a, Å	9.1630(3)	9.0278(2)
b, Å	12.5772(4)	12.6317(3)
c, Å	7.3398(2)	7.2353(2)
V, $Å^3$	845.87(4)	825.09(4)
Z	4	4
ρ_{calc}, g/cm^3	1.931	1.980
λ, Å	0.710 73	2.0775
μ, mm^{-1}	2.150	N/A
$R(F)^a$	0.0200	0.0106
$R_w(F)^b$	0.0486	0.0130
GOF	1.082	1.05

$^aR = \sum||F_o| - |F_c||/\sum|F_o|$. $^bR_w = [\sum w[|F_o| - |F_c|]^2/\sum w[|F_o|^2]^{1/2}$.

Table 2. Selected Bond Lengths (Å) and Angles (deg) for $MnCl_2(urea)_2$ at 295 and 1.4 K

bond or angle	X-rays (295 K)	neutrons (1.4 K)
Mn−Cl	2.5864(6)	2.540(13)
Mn−Cl#[a]	2.6004(7)	2.622(13)
Mn−O	2.119(1)	2.134(6)
O−C	1.256(2)	1.220(7)
C−N(1)	1.330(3)	1.357(7)
C−N(2)	1.326(3)	1.381(6)
N(1)−H(1)	0.882	0.97(3)
N(1)−H(2)	0.877	1.06(2)
N(2)−H(3)	0.877	1.06(2)
N(2)−H(4)	0.880	0.90(3)
O−Mn−O#	176.3(1)	173.5(10)
O−Mn−Cl	85.94(6)	86.4(4)
O−Mn−Cl#	88.06(5)	88.0(4)
Cl−Mn−Cl#	90.27(3)	89.44(11)
Mn−O−C	135.4(1)	134.9(4)
O−C−N(1)	120.2(2)	120.3(5)
N(1)−C−N(2)	118.3(2)	116.9(5)

[a]Symmetry code: # = −*x*, 1 − *y*, *z*.

Table 3. Interchain Hydrogen Bond Distances and Angles

D−H···A	D−H (Å)	H···A (Å)	D···A (Å)	D−H···A ∠ (deg)
		X-rays (295 K)		
N1−H2···Cl	0.88	2.65	3.461(2)	154
N2−H4···O	0.88	2.11	2.917(2)	152
		Neutrons (1.4 K)		
N1−H2···Cl	1.06(2)	2.49	3.43	148
N2−H4···O	0.89(3)	2.06	2.84	145

Pulsed-Field Magnetization. Measurements up to 60 T were made at the Pulsed-Field Facility of the National High Magnetic Field Facility using a 1.5 mm bore, 1.5 mm long, 1500-turn compensated-coil susceptometer, constructed from 50-gauge high-purity copper wire.[19a] When a sample is within the coil, the signal voltage *V* is proportional to (d*M*/d*t*), where *t* is the time. Numerical integration of *V* is used to evaluate *M*. The sample is mounted within a 1.3 mm diameter ampule that can be moved in and out of the coil. Accurate values of *M* are obtained by subtracting empty coil data from that

DOI: 10.1021/acs.inorgchem.5b02162
Inorg. Chem. XXXX, XXX, XXX−XXX

measured under identical conditions with the sample present. The susceptometer was placed inside a ^{3}He cryostat providing temperatures down to 0.5 K. The field B was measured by integrating the voltage induced in a 10-turn coil that was calibrated by observing the de Haas–van Alphen oscillations of the belly orbits of the copper coils of the susceptometer.

Neutron Scattering. Diffraction studies were made using the 32-detector high-resolution BT-1 powder diffractometer located at the NIST Center for Neutron Research (NCNR, Gaithersburg, MD). A neutron wavelength of 2.0775 Å produced by a Ge(311) monochromator was used. Collimators with horizontal divergences of 15′, 20′, and 15′ full-width-at-half-maximum (fwhm) were used for the in-pile, monochromatic and diffracted beams, respectively. Intensities were measured in steps of 0.05° 2θ between 3° and 165° at temperatures of 1.4 and 5 K, i.e., below and above T_N. A hydrogenated powder sample of $MnCl_2(urea)_2$ weighing approximately 2 g was loaded into a vanadium can, mounted in a Janis top-loading ^{3}He cryostat and positioned in the center of the neutron beam. Nuclear and magnetic structure refinements were performed using GSAS.[20] Initial atomic positions, including H atoms, were taken from the single-crystal X-ray structure and then freely refined. The magnetic-order parameter was deduced using a series of scans obtained in temperature increments of roughly 0.1 K between 1.4 and 5 K.

Inelastic neutron scattering measurements were performed at 1.6 and 5 K on the same sample of $MnCl_2(urea)_2$ using the Fermi chopper time-of-flight spectrometer also located at the NCNR. The sample was contained within a 1-cm diameter Al can backfilled with ^{4}He exchange gas. The temperature was controlled using a flow-type pumped-liquid ^{4}He cryostat. The neutron wavelength for the measurement was fixed at 6 Å, which results in a measured elastic energy resolution fwhm of 0.07 meV. Data were collected for approximately 6 h at each temperature. For the neutron data, uncertainties are statistical in origin and represent one standard deviation.

RESULTS AND DISCUSSION

Crystal Structure. The structure of $MnCl_2(urea)_2$ was investigated at 295, 5, and 1.4 K using a combination of single-crystal X-ray and neutron powder-diffraction measurements. In the *Iba*2 space group, the Mn(II) ion has 2-fold rotation symmetry about the crystallographic c-axis, occupying Wyckoff position 4b. All other atoms occupy general positions. As shown in Figure 1, each Mn(II) ion is six-coordinate with four

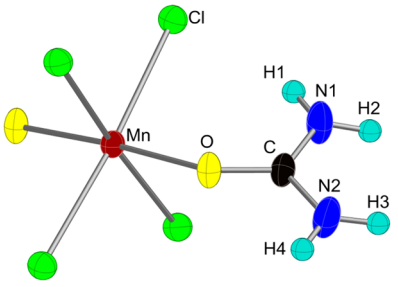

Figure 1. Crystal structure of $MnCl_2(urea)_2$ determined by single-crystal X-ray and powder neutron diffraction data, showing the asymmetric unit and atom labeling scheme. Thermal displacement parameters are drawn for room temperature at the 35% probability level.

Cl^- occupying the equatorial plane [Mn–Cl = 2.5864(6) and 2.6004(7) Å] while two oxygen atoms [Mn–O = 2.119(1) Å] from urea ligands reside on the axial positions. The $MnCl_4O_2$ octahedron is rather distorted from ideal octahedral symmetry with the largest deviations being 85.94(6)° and 175.23(2)° for O–Mn–Cl and Cl–Mn–ClC, respectively. The chloride ions link the Mn centers into linear chains (Figure 2) along the c-direction with Mn···Mn separations of 3.670 Å which is one-

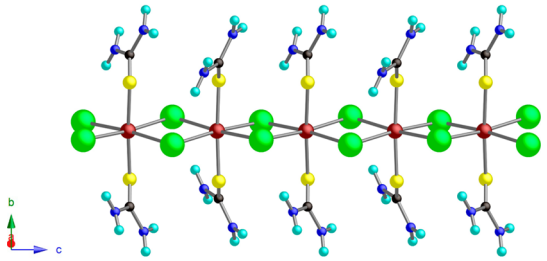

Figure 2. Segment of a linear chain for $MnCl_2(urea)_2$. The atom labeling scheme is given in Figure 1.

half of the c lattice parameter. Each Cl^- bridge makes nearly orthogonal Mn–Cl–Mn bond angles of 90.07(1)°. Binuclear $[Mn_2Cl_4(tacud)_2]$ (tacud = 1,4,8-triazacycloundecane) contains a bridge angle of 90.2°.[12a]

The rhombic Mn_2Cl_2 core encountered in $MnCl_2(urea)_2$ is common to several other binuclear and chain-type Mn(II)-chloride complexes, including $[Mn_2Cl_4(tacud)_2]$,[12a] $MnCl_2\cdot 2H_2O$,[3] $MnCl_2(2,2'\text{-bipy})$ (bipy = bipyridine),[9] $MnCl_2$(mppma) [mppma = *N*-(3-methoxy-propyl)-*N*-(pyridine-2-ylmethyl)amine],[21] and $MnCl_2(pz)_2$ (pz = pyrazole).[22] The corresponding Mn···Mn distance/Mn–Cl–Mn bond angle in the dihydrate, mppma, and bipy complexes are 3.691 Å/92.55°, 3.790 Å (average)/94.14°, and 3.835 Å/96.4°. These Mn···Mn distances are shorter than that found in polymeric $MnCl_2$(tmen) (tmen = *N*,*N*,*N*′,*N*′-tetramethylethylenediamine)[23] which is consistent with a slightly larger Mn–Cl–Mn bond angle. Adjacent rhomboids along the Mn–Cl_2–Mn chains in $MnCl_2(urea)_2$ are alternately tilted by 6.6° (see Figure 3a).

The crystal packing in $MnCl_2(urea)_2$ is unique as the chains do not stagger as typically observed in structures of this type.[3,21,22] Instead, neighboring chains pack in-registry and are linked into an intricate three-dimensional (3D) network via N–H···Cl and N–H···O hydrogen bonds as illustrated in Figure 3a,b with relevant distances given in Table 3. This packing arrangement provides interchain Mn···Mn separations of 7.780 and 8.601 Å along the face-diagonal of the ab-plane and body-diagonals of the unit cell, respectively. In comparing the 295 K single-crystal X-ray data with 1.4 K neutron powder data for $MnCl_2(urea)_2$ we find a lattice contraction along the a- and c-axes and expansion along b. We attribute the b-axis change to a strengthening of the N–H···Cl hydrogen bond interaction as evidenced by shortening of the H···Cl distance.

Magnetic Susceptibility, $\chi(T)$. The bulk magnetic susceptibility of $MnCl_2(urea)_2$ has been investigated between 2 and 300 K; data are shown in Figure 4. $\chi(T)$ increases gradually upon cooling until a broad maximum (T_{max}) is reached at 9 K. Upon cooling further down to 2 K, $\chi(T)$ gradually decreases and then rises slightly. This small increase in the susceptibility could be due to a trace amount of paramagnetic impurity. The broad maximum, however, is attributed to short-range magnetic ordering between $S = {}^5/_2$ Mn(II) ions along the bibridged chains. The $\chi(T)$ data were fit between 50 and 300 K to a Curie–Weiss law, $\chi = Ng^2\mu_B{}^2S(S+1)/3k_B(T-\theta)$, where θ is the Weiss constant and the remaining symbols have their usual meaning.[24] The resulting fit gave a slightly anisotropic g-value of 2.027(1) and $\theta = -17.7(3)$

DOI: 10.1021/acs.inorgchem.5b02162
Inorg. Chem. XXXX, XXX, XXX–XXX

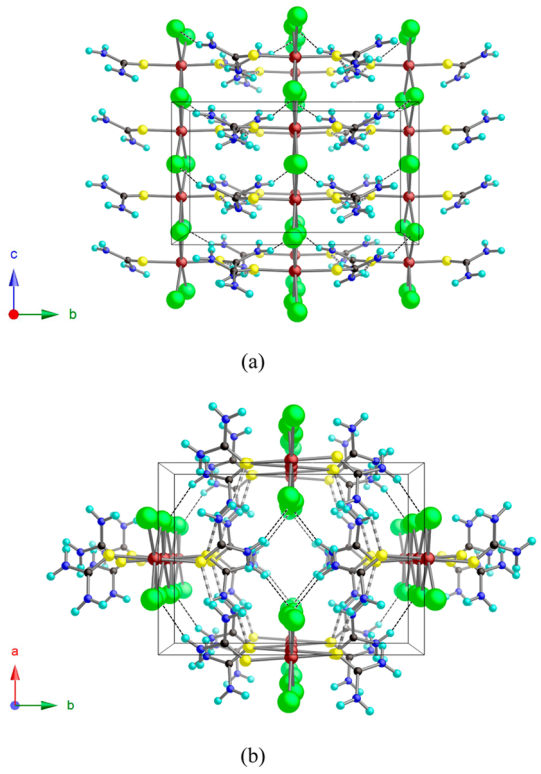

Figure 3. Chain packing diagrams for $MnCl_2(urea)_2$ viewed along the (a) *a*-axis and (b) *c*-axis. Note the successive tilting of adjacent $MnCl_4O_2$ octahedra along the chain *c*-axis. The atom labeling scheme is given in Figure 1. Cylindrical and dashed lines indicate N−H···O and N−H···Cl hydrogen bonds, respectively, as described in the text.

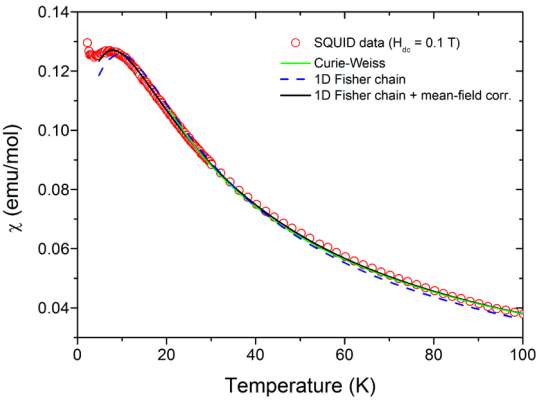

Figure 4. Magnetic susceptibility data for a powder sample of $MnCl_2(urea)_2$ for T < 100 K. Solid and dashed lines delineate theoretical fits of $\chi(T)$ to Curie−Weiss and 1D Fisher chain models as described in the text. Note that 1 emu = 10^{-3} A m^2.

K, where a negative θ-value specifies antiferromagnetic (AFM) coupling between Mn(II) spins. Since spin−orbit coupling is largely quenched in high-spin, six-coordinate Mn(II) complexes, as found in $MnCl_2(urea)_2$ and many related systems, the obtained θ-value is almost entirely attributable to magnetic interactions between metal centers. We caution, however, that a small zero-field splitting could result due to even the slightest structural distortion about the metal center.

Considering that the crystal structure consists of uniformly spaced Mn(II) ions arranged as chemical chains, we first attempted to fit the $\chi(T)$ data to a classical-spin Fisher AFM chain model ($H = J\Sigma S_i \cdot S_j$ with $J > 0$ being assigned to AFM interactions) to obtain the intrachain exchange constant (J). In a second attempt, and to account for possible interchain couplings (J'), we included a mean-field correction term.[25,26] In each case, a least-squares fit of the data between 5 and 300 K, which excluded any single-ion anisotropy (D), yielded g = 2.03(2) and J = 2.3(1) K for the Fisher chain model (dashed blue line in Figure 4) and g = 2.03(2), J = 1.9(1) K, and zJ' = −0.1(1) K for the Fisher chain plus MF model (solid black line in Figure 4). A mean-field approach is often invoked to explain residual magnetic interactions; however, in a later section, we describe a more reliable method to determine multiple magnetic parameters in a bulk material such as $MnCl_2(urea)_2$ using inelastic neutron scattering.

The low dimensionality of the spin system can be further gleaned from the expression $k_B T_{max}/J = 1.12S(S+1) + 0.10$, to estimate J.[27] The J obtained from this equation is 2.2 K and consistent with the fitted J-values. As compared to other bibridged Mn(II) chains listed in Table 4, the J for $MnCl_2(urea)_2$ is larger. While the Mn−Cl−Mn bridge angle in $MnCl_2(urea)_2$ is ∼90° and presents the largest AFM interaction among related materials, magnetostructural trends are difficult to rationalize; the binuclear compound $[Mn_2Cl_4(tacud)_2]$[12a] has a very similar Mn_2Cl_2 core as compared to the urea compound, and J was determined to be 5.2 K.

Table 4. Summary of Magnetic Data for Selected $S = {}^5/_2$ Bibridged Mn(II)-Chloride Chains[a]

compd[b]	Mn−Cl−Mn bridge angle (deg)	J/k_B (K)[c]	ref
$MnCl_2 \cdot 2H_2O$	∼90	0.45	3
$MnCl_2$(mppma)	94.1	0.36	21
$MnCl_2$(tmen)	80.0, 93.7, 94.1, 100.0, 106.5, 169.9	∼ 0	23
$MnCl_2$(2,2′-bipy)	96.4	−0.27	9
$MnCl_2$(4,4′-bipy)	92.2	N/A	10
$MnCl_2$(4-CNpy)$_2$	93.5	0.8	37
$MnCl_2$(H_2dapd)	99.5	−0.29	38
$MnCl_2(urea)_2$	90.1 (295 K), 89.2 (1.4 K)	1.9,[d] 2.22[e]	this work

[a]Given J-values are based on a Heisenberg 1D model for which $J > 0$ corresponds to AFM coupling. [b]Chemical abbreviations: mppma = *N*-(3-methoxy-propyl)-*N*-(pyridine-2-ylmethyl)amine; tmen = *N*,*N*,*N*′,*N*′-tetramethylethylenediamine; bipy = bipyridine; CNpy = cyanopyridine; H_2dapd = 2,6-diacetylpyridinedioxime. [c]It is quite possible that some of these previously reported J values may in fact be 2J. [d]Obtained from the fit of $\chi(T)$ to the Fisher chain model incorporating a mean-field term as described in the text. [e]Intrachain J as determined from the INS study.

Of significance is that the g-values obtained from both magnetic models slightly exceed the expected free electron value of 2.0023. This points to a possible single-ion anisotropy arising from a splitting of the six magnetic sublevels of the $S = \pm{}^5/_2$ ground state in zero-field (D).[28] For instance, in a series of mononuclear complexes MnX_2(tpa) (tpa = tris-2-picolylamine), D was found to be 0.17, −0.50, and −0.84 K for X = Cl, Br, and I, respectively.[29] Granted, these compounds consist of MnN_4Cl_2 sites, as opposed to MnN_2Cl_4 found in $MnCl_2(urea)_2$; however, the important feature is that D is finite.

High-Field Magnetization. Figure 5a shows the magnetization $M(H)$ of $MnCl_2(urea)_2$ measured in pulsed magnetic fields at four different temperatures; corresponding differential susceptibility (dM/dH) plots are shown in the lower panel.

DOI: 10.1021/acs.inorgchem.5b02162
Inorg. Chem. XXXX, XXX, XXX−XXX

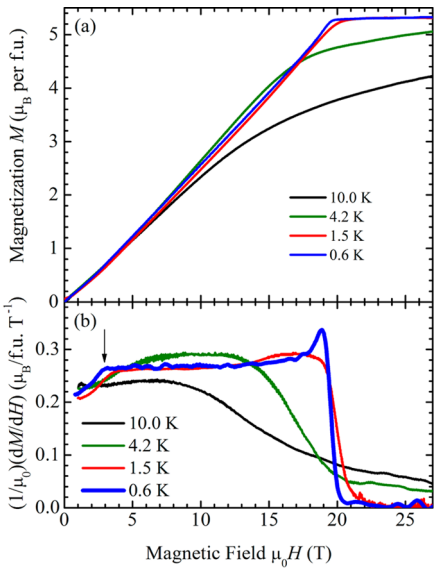

Figure 5. (a) Pulsed-field magnetization data obtained for a powder sample of $MnCl_2(urea)_2$, calibrated by comparison with vibrating-sample magnetometer data at similar temperatures. (b) Differential susceptibility (dM/dH) curves derived from the data in part a. The arrow in part b indicates the feature in the 0.6 K magnetization data at 2.8 T, suggestive of a spin-flop or metamagnetic-like transition at this field.

Many similar studies have been carried out on $S = {}^1/_2$ and $S = 1$ quantum magnets.[19] In those low-spin (compared to Mn) systems, low-temperature $M(H)$ data exhibit a concave (i.e., gradual steepening with increasing field) curve before a relatively sudden saturation at a well-defined magnetic field.[19] In general, the lower the effective magnetic dimensionality, the more concave the data, a behavior that has been modeled successfully using a quantum-Monte Carlo approach.[19] By contrast, the lowest temperature $M(H)$ data for $MnCl_2(urea)_2$ exhibit a constant gradient from 2.8 T up to just below the saturation field. This is followed by a small increase in gradient close to saturation and then a rapid fall to zero as the moments become aligned (Figure 5b, blue curve). In the context of the $S = {}^1/_2$ and $S = 1$ systems, such behavior would suggest isotropic (three-dimensional) exchange interactions. However, similar approaches to saturation have been observed in a wide variety of Mn complexes, including MOFs in which the Mn ions populate small, magnetically isolated clusters[30] and crystalline organic magnets known to be quasi-one- or two-dimensional considering spatial exchange anisotropy.[31] In all of these Mn(II) compounds, it seems that the large number of possible spin projections of the Mn(II) ions circumvents the geometrical restrictions caused by reduced dimensionality that dictates the approach to saturation in the low-spin complexes; thus, the almost-linear low-temperature $M(H)$ until just below saturation, followed by a brief increase in gradient and a rapid fall in gradient to zero (Figure 5a,b), is "universal" behavior in metal−organic magnets featuring ions such as Mn(II).[32] From conventions established earlier,[19] the saturation field is chosen as the midpoint of the sharp fall to zero observed in the lowest-temperature dM/dH plot (Figure 5b, blue curve), yielding a value of 19.6 T.

In addition to the low-temperature, almost linear approach to saturation (Figure 5a, $T = 0.6$ K data), there is a sharp change in gradient at 2.8 T (Figure 5b, blue curve, indicated by an arrow). This suggests some form of metamagnetic transition, i.e., a field-driven reconfiguration of the low-field ground state. Increasing the temperature to 1.5 K (Figure 5b, red curve) broadens and shifts this feature up in field by a small amount; by 4.2 K, it is no longer visible (Figure 5b, green curve).

The saturation magnetization of 5.3 ± 0.2 μ_B per formula unit (Figure 5a) suggests that the Mn(II) ions contribute their full moment at high fields, in contrast to the reduced moment extracted above from the low-field data. In addition, the saturation field represents the point at which the magnetic energy of the spins finally overcomes the exchange interactions; with knowledge of the g-factor one can extract the effective exchange energy acting on the Mn(II) ions.[19] Assuming a chain-like configuration (two nearest neighbors) and using the g-factor given above, the saturation field of 19.6 T yields an effective $J = 2.6$ K. This is close to, but slightly higher than, the individual exchange energies derived below from the inelastic neutron scattering study (see below).

In the section on analysis of neutron diffraction data, we describe how a portion of the Mn(II) spin-density probably diffuses onto the polarizable Cl^- ligands at zero magnetic field. This acts to reduce both the effective exchange energies and magnetic moment available from the Mn(II) ions. Therefore, the metamagnetic-like transition at 2.8 T likely represents a rearrangement of the Cl^- ligand spins that results in a slightly higher effective exchange energy and recovery of the full Mn(II) moment.

Zero-Field Magnetic Structure. A comparison of neutron diffraction patterns made at 1.4 and 5 K, the latter not shown, reveals several additional Bragg peaks at the lower temperature (Figure 6) that are magnetic in origin. These additional peaks,

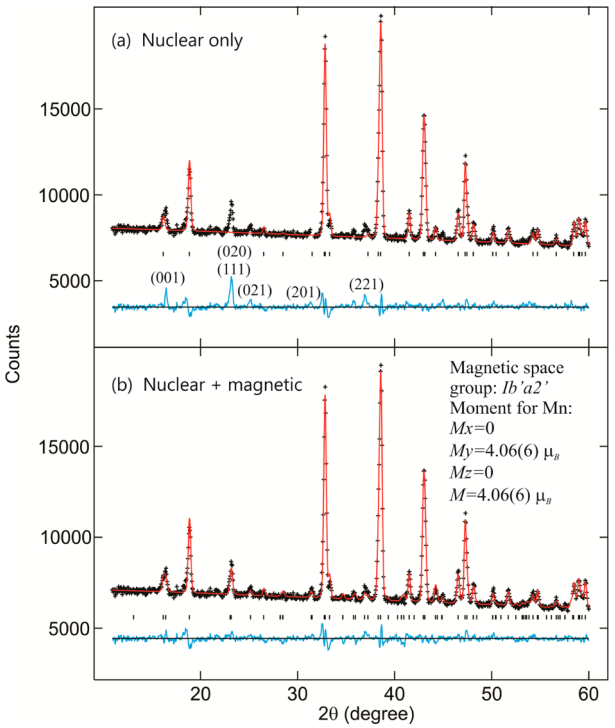

Figure 6. Neutron diffraction pattern obtained at 1.4 K temperature, well below $T_N = 3.1$ K, showing the difference between the (a) nuclear-only well above T_N and (b) nuclear + magnetic models. Residual peaks of magnetic origin are indexed in the difference plot of part a.

DOI: 10.1021/acs.inorgchem.5b02162
Inorg. Chem. XXXX, XXX, XXX−XXX

indexed as (001), (020) or (111), (021), (201), and (221), are a result of long-range AFM order in the material. Rietveld profile analysis of the 1.4 K data yielded a propagation vector (τ) of [0, 0, 0] indicating that the magnetic and nuclear unit cells are equivalent.

The magnetic structure (Figure 7) of $MnCl_2(urea)_2$ can be rationalized in the following manner: (1) Along the chain,

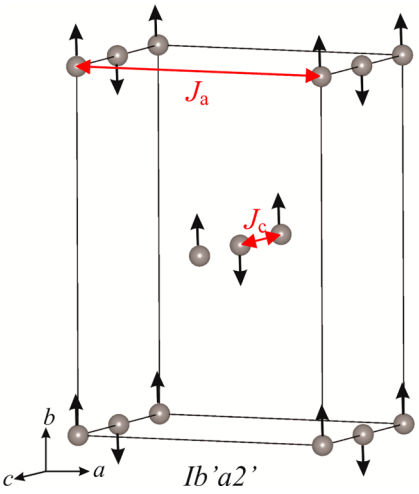

Figure 7. Zero-field magnetic structure of $MnCl_2(urea)_2$ as determined from powder neutron diffraction. The bibridged Mn–Cl_2–Mn chains run parallel to the crystallographic *c*-axis with the collinear magnetic moments aligned along the *b*-axis.

Mn(II) magnetic moments align antiparallel relative to adjoining neighbors, i.e., are antiferromagnetic. (2) The Mn(II) moments that lie on the vertices of the unit cell align ferromagnetically relative to the chain running through the body center. (3) The total magnetic moment, M_T, per Mn(II) ion is 4.06(6) μ_B which is the vector sum of the spatial components $M_x = M_z = 0$ and $M_y = 4.06(6)$ μ_B. The determined M_T value is reduced by ~1 μ_B from the expected value of 5 μ_B for isotropic high-spin $S = {}^5/_2$ Mn(II). This observation could arise if a portion of the Mn(II) spin density was diffused onto the polarizable Cl^- ligands. Should this occur, each Cl would bear a magnetic moment of roughly 0.13 μ_B and be aligned antiparallel to the Mn(II) moment, which is ~3% of M_T. This is not unreasonable in that ~5% of the Ir(IV) magnetic moment is delocalized onto the Cl's in K_2IrCl_6 due to covalency effects, for example.[33] For $MnCl_2(urea)_2$ in zero-field, the net effect would be cancellation of the Cl magnetic moments since each Cl is shared by two antiparallel Mn, which is consistent with the lack of such evidence from the BT-1 data. Presumably, in high magnetic fields the Cl moments would reorient in a parallel form (possibly by 2.8 T because this corresponds to ~14% of B_{sat}, i.e., ~0.8 μ_B), thus possibly explaining the larger total moment observed in the high-field magnetization data. Of note is that the presence of quantum fluctuations in $MnCl_2(urea)_2$, as needed to reduce the size of the experimentally observed ordered moment, is inconceivable for $S = {}^5/_2$.

To determine the Néel temperature, the intensity of the (111) magnetic peak was monitored as a function of temperature as shown in Figure 8. From the plot it can be seen that the peak intensity becomes invariant for temperatures above approximately 3 K. We fit these data in two ways. First, we use a power-law of the form $I(T) = A + B(T_N - T)^{2\beta}$ for T

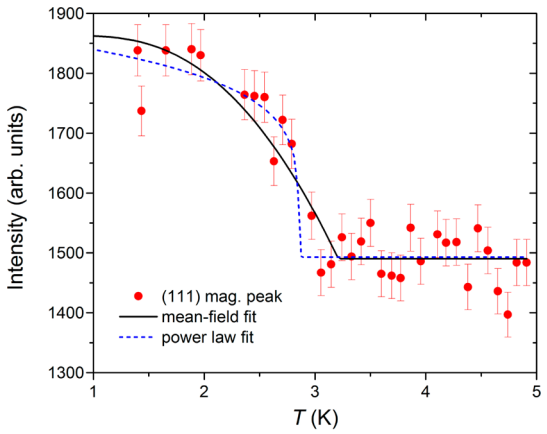

Figure 8. Temperature dependence of the (111) magnetic Bragg peak obtained from the BT-1 powder diffractometer. The solid and dashed lines correspond to mean-field and power law fits as described in the text.

< T_N, where the value A accounts for the background and β is the critical exponent. For $T > T_N$ the data were fit to obtain the A value. From Figure 8, this comparison results in a good representation of the measurement with $\beta = 0.19(7)$ and $T_N = 2.99(4)$ K. While β is consistent with magnetic interactions of reduced dimensionality, we caution that it is only meaningful in the critical region. Second, we use mean-field theory ($\beta = 0.5$) for comparison which gives $T_N = 3.2(1)$ K. Of consequence is that the mean-field fit is flat all the way down to $T = 0$ whereas the power law fit continues to increase slightly. In common, however, is that neither fit satisfactorily accounts for the missing ordered moment outside of the uncertainty.

Inelastic Neutron Scattering. Figure 9 shows the measured wave-vector (Q) integrated scattering intensity as a

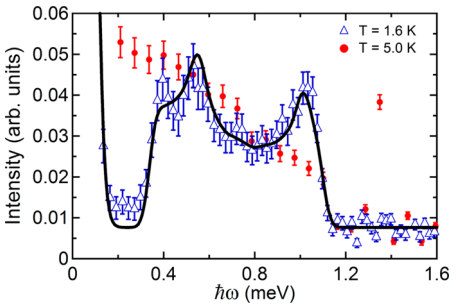

Figure 9. (a) Wave-vector integrated scattering intensity as a function of energy transfer for $MnCl_2(urea)_2$ at $T = 1.6$ and $T = 5.0$ K. The solid line is the result of the powder averaged linear spin-wave theory discussed in the text. An elastic Gaussian peak is included in the fit to account for the incoherent nuclear scattering. Details of the measurement and fitting procedure are discussed in the text. The single high point at $\hbar\omega = 1.35$ meV is much sharper than the instrumental energy resolution and is spurious scattering.

function of neutron energy transfer, $\hbar\omega$. The $T = 1.6$ K data exhibit a band of excitations between approximately 0.4 and 1.1 meV. Upon heating to $T = 5$ K, these excitations broaden out substantially, with the paramagnetic scattering becoming diffusive (quasielastic) in nature. The range of scattering angles available with the Fermi chopper spectrometer ranges between 5° and 140°. For the band of excitations observed at $T = 1.6$ K, this range of scattering angle corresponds to an approximate range 0.17–1.83 $Å^{-1}$ in wave-vector transfer. These low Q

DOI: 10.1021/acs.inorgchem.5b02162
Inorg. Chem. XXXX, XXX, XXX–XXX

values, together with the temperature dependence, clearly indicate that this scattering is magnetic. There are three individual peaks that make up the broader distribution of magnetic scattering. Two correspond to the top and bottom of the magnon density-of-states. In the following, we show that these local maxima can be used to constrain the exchange constants in $MnCl_2(urea)_2$.

At 1.6 K, $MnCl_2(urea)_2$ is within the bulk ordered magnetic phase. Accordingly, we analyze the measured magnetic spectrum using linear spin-wave theory based upon the pedagogical Heisenberg Hamiltonian that includes single-ion anisotropy, D (eq 1)

$$H = \sum_{\alpha} \sum_{\langle i,j \rangle \alpha} J_{\alpha} S_i \cdot S_j + \sum_i D(S_z^2)_i \quad (1)$$

where α is summed over the a, b, and c axes; we define the y-axis to be parallel to the ordered moment.[34] On the basis of the ordered magnetic structure shown in Figure 7, we consider the moments to point along the (110) axis of the crystal. Although single-crystal inelastic neutron scattering is the preferred method for extracting exchange parameters based upon measured dispersion curves,[34] we are able to use the powder measurement to determine the primary exchange interactions in $MnCl_2(urea)_2$. For $T < T_N$, the gap in the magnon density of states is due to D. We consider the dominant exchange interaction based upon the crystal structure to be along the crystallographic c-axis, J_c. The next largest exchange interaction is most likely J_a, since the distance between Mn(II) sites along the a-axis is the next shortest in the crystal structure at 9.16 Å. This results in the spin-wave dispersion (eqs 2−4)

$$A_Q = 2S\{J_a[\cos(2\pi H) - 1] + J_c - D\} \quad (2)$$

$$B_Q = 2S[J_c \cos(\pi L)] \quad (3)$$

$$\hbar\omega(Q) = \sqrt{A_Q^2 - B_Q^2} \quad (4)$$

where S is the magnitude of the spin, J_c is the antiferromagnetic exchange along the chain-axis, and J_a is a ferromagnetic nearest neighbor exchange along the a-axis.[35] We powder-average the calculated scattering intensity associated with a linear spin wave cross-section for the dispersion in eqs 2−4.[36] The B_Q term has a $\cos(\pi L)$ factor due to there being two Mn(II) moments oriented along the c-axis of the unit cell. The spectrum is then integrated for the measured range of wave-vectors, convolved with a Gaussian with the same width as the elastic energy resolution, and compared to the measured scattering intensity. We fix the background and only include a multiplicative prefactor in this fitting procedure. By performing this calculation over a range of J_a, J_c, and D space we are able to determine the minimum value of reduced χ^2. The fitted range of data used to determine the exchange constants was between 0.32 and 1.23 meV in energy transfer. The determined line shape shown in Figure 9 is based upon the best fit parameters of $J_c = 0.191(5)$ meV (~2.22 K), $D = -0.012(3)$ meV (~−0.14 K), and $J_a = -0.009(2)$ meV (~−0.10 K) with a reduced χ^2 of 0.887 indicating an excellent fit. The signs of J_a and J_c are in keeping with those used in the previous Hamiltonian used to model the magnetic susceptibility data. Error bars for an individual variable are based upon fixing the other variables and determining at what value the reduced χ^2 increases by 1. The value of J_c is larger than the other exchange constants in this compound by more than a factor of 10, and it is the quasi-1D nature of $MnCl_2(urea)_2$ that is responsible for the sharp magnetic density of states at the top and bottom of the spectrum. The additional peak in the spectrum at approximately 0.5 meV is attributed to weaker interchain interactions.

The calculated wave-vector-dependent dispersion has local minima at (h00), (00l), and (h0l) positions for integer h and l values. These values correspond to the locations of the magnetic peaks observed in the diffraction data, as expected for this magnetic structure.

The distance between moments along the c-axis is small such that the next-nearest neighbor (nnn) distance along the c-axis (7.338 Å) is shorter than the nearest-neighbor distance between moments along the a-axis (9.163 Å). The powder inelastic neutron scattering measurement is able to identify the significant exchange interactions, but cannot distinguish the possibility of a nonzero *nnn* exchange along the c-axis. Likewise the exchange interaction along the (1 0 ±0.5) direction may be comparable to J_a but would require INS measurements on single crystals to verify. In turn, these additional exchange interactions would likely be frustrated. Adding additional interactions along other potential exchange paths did not improve the comparison with the data with any statistical significance. These would be of a smaller magnitude than the J_a we determined and potentially contribute to some degree of geometric frustration in this compound.

CONCLUSIONS

We employed X-ray and neutron scattering techniques along with susceptibility and high-field magnetization data to determine the crystal structure and microscopic magnetic properties of the coordination polymer $MnCl_2(urea)_2$. A quasi-1D chain structure was found with Mn(II) sites packed in close proximity along the c-axis. A combination of magnetic neutron diffraction and inelastic neutron scattering measurements confirms the existence of AFM coupled $S = {}^5/_2$ moments along the c-axis of the crystal structure. $MnCl_2(urea)_2$ orders at a temperature of 3 K such that three-dimensional magnetic interactions ultimately contribute to the exchange interactions in the system, even though the intrachain interaction is an order-of-magnitude larger and dominates the magnetic behavior. This compound represents an unusual classical-spin chain displaying *intrachain* AFM and *interchain* FM interactions, the latter being contrary to the usual observation. A field-dependent phase transition occurs at 2.8 T with the fully polarized state being realized at 19.6 T. Examining other metal−organic crystal structures based upon the urea ligand are likely to further contribute to our general understanding of structural influences on the magnetic properties of materials of this type.

ASSOCIATED CONTENT

Supporting Information

The Supporting Information is available free of charge on the ACS Publications website at DOI: 10.1021/acs.inorgchem.5b02162.

Crystallographic data (CIF)

AUTHOR INFORMATION

Corresponding Author

*E-mail: jmanson@ewu.edu. Phone: (509) 359-2878. Fax: (509) 359-6973.

DOI: 10.1021/acs.inorgchem.5b02162
Inorg. Chem. XXXX, XXX, XXX−XXX

Notes

The authors declare no competing financial interest.

■ ACKNOWLEDGMENTS

The work at EWU was supported by the National Science Foundation (NSF) under Grant DMR-1306158. J.L.M. thanks Prof. Jesper Bendix for helpful discussions. We acknowledge the support of the National Institute of Standards and Technology (NIST), U.S. Department of Commerce, in providing their neutron research facilities used in this work; identification of any commercial product or trade name does not imply endorsement or recommendation by NIST. Work performed at the National High Magnetic Field Laboratory, USA, was supported by the National Science Foundation Cooperative Agreement DMR-1157490, the State of Florida, and the U.S. Department of Energy (DoE), and through the DoE Basic Energy Science Field Work Proposal "Science in 100 T." The research at ORNL was sponsored by the Scientific User Facilities Division, Office of Basic Energy Sciences, U.S. Department of Energy.

■ REFERENCES

(1) See, for example: (a) Lapidus, S. H.; Manson, J. L.; Park, H.; Clement, A. J.; Ghannadzadeh, S.; Goddard, P. A.; Lancaster, T.; Moeller, J. S.; Blundell, S. J.; Telling, M. T. F.; Kang, J.; Whangbo, M.-H.; Schlueter, J. A. *Chem. Commun.* **2013**, *49*, 499−501. (b) Prescimone, A.; Morien, C.; Allan, D.; Schlueter, J. A.; Tozer, S.; Manson, J. L.; Parsons, S.; Brechin, E. K.; Hill, S. *Angew. Chem., Int. Ed.* **2012**, *51*, 7490−7494. (c) Wang, C. H.; Lumsden, M. D.; Fishman, R. S.; Ehlers, G.; Hong, T.; Tian, W.; Cao, H.; Podlesnyak, A.; Dunmars, C.; Schlueter, J. A.; Manson, J. L.; Christianson, A. D. *Phys. Rev. B: Condens. Matter Mater. Phys.* **2012**, *86*, 064439. (d) Musfeldt, J. L.; Liu, Z.; Li, S.; Kang, J.; Lee, C.; Jena, P.; Manson, J. L.; Schlueter, J. A.; Carr, L. G.; Whangbo, M.-H. *Inorg. Chem.* **2011**, *50*, 6347−6352. (e) Halder, G. J.; Chapman, K.; Schlueter, J. A.; Manson, J. L. *Angew. Chem., Int. Ed.* **2011**, *50*, 419−421. (f) Pratt, F. L.; Baker, P. J.; Blundell, S. J.; Lancaster, T.; Ohira-Kawamura, S.; Baines, C.; Shimizu, Y.; Kanoda, K.; Watanabe, I.; Saito, G. *Nature* **2011**, *471*, 612−616. (g) Awwadi, F.; Willett, R. D.; Twamley, B.; Schneider, R.; Landee, C. P. *Inorg. Chem.* **2008**, *47*, 9327−9332. (h) Shapiro, A.; Landee, C. P.; Turnbull, M. M.; Jornet, J.; Deumal, M.; Novoa, J. J.; Robb, M. A.; Lewis, W. *J. Am. Chem. Soc.* **2007**, *129*, 952−959. (i) Zeleňák, V.; Orendáčová, A.; Cisarová, I.; Černák, J.; Kravchyna, O. V.; Park, J.-H.; Orendáč, M.; Anders, A. G.; Feher, A.; Meisel, M. W. *Inorg. Chem.* **2006**, *45*, 1774−1782. (j) Calvo, R.; Passeggi, M. C. G.; Moreno, N. O.; Barberis, G. E.; Chaves, A. B.; Torres, B. C. M.; Lezama, L.; Rojo, T. *Phys. Rev. B: Condens. Matter Mater. Phys.* **1999**, *60*, 1197−1203. (k) Yamashita, M.; Manabe, T.; Inoue, K.; Kawashima, T.; Okamoto, H.; Kitagawa, H.; Mitani, T.; Toriumi, K.; et al. *Inorg. Chem.* **1999**, *38*, 1894−1899.

(2) (a) Seki, S.; Kurumaji, T.; Ishiwata, S.; Matsui, H.; Murakawa, H.; Tokunaga, Y.; Kaneko, Y.; Hasegawa, T.; Tokura, Y. *Phys. Rev. B: Condens. Matter Mater. Phys.* **2010**, *82*, 064424. (b) Zhao, L.; Hung, T.-L.; Li, C.-C.; Chen, Y.-Y.; Wu, M.-K.; Kremer, R. K.; Banks, M. G.; Simon, A.; Whangbo, M.-H.; Lee, C.; Kim, J. S.; Kim, I.; Kim, K. H. *Adv. Mater.* **2012**, *24*, 2469−2473.

(3) (a) McElearney, J. N.; Merchant, S.; Carlin, R. L. *Inorg. Chem.* **1973**, *12*, 906−908. (b) DeFotis, G. C.; Kim, M. G.; Reed, Z. D.; Chan, D. G.; Hopkinson, A. T.; Matsuyama, Y. *Phys. Rev. B: Condens. Matter Mater. Phys.* **2006**, *73*, 214434.

(4) (a) Tun, Z.; Buyers, W. J. L.; Armstrong, R. L.; Hirakawa, K.; Briat, B. *Phys. Rev. B: Condens. Matter Mater. Phys.* **1990**, *42*, 4677−4681. (b) Janke, E.; Hutchings, M. T.; Day, P.; Walker, P. J. *J. Phys. C: Solid State Phys.* **1983**, *16*, 5959−5968. (c) Als-Nielsen, J.; Bramwell, S. T.; Hutchings, M. T.; McIntyre, G. J.; Visser, D. *J. Phys.: Condens. Matter* **1993**, *5*, 7871−7892. (d) Rauh, H.; Erkelens, W. A. C.; Regnault, L. P.; Rossat-Mignod, J.; Kullman, W.; Geick, R. *J. Phys. C: Solid State Phys.* **1986**, *19*, 4503−4510.

(5) (a) Haynes, J. S.; Sams, J. R.; Thompson, R. C. *Inorg. Chem.* **1986**, *25*, 3740−3744. (b) Carlin, R. L.; Carnegie, D. W.; Bartolome, J.; Gonzalez, D.; Floria, L. M. *Phys. Rev. B: Condens. Matter Mater. Phys.* **1985**, *32*, 7476−7482.

(6) Schlueter, J. A.; Park, H.; Halder, G. J.; Armand, W. R.; Dunmars, C.; Chapman, K. W.; Manson, J. L.; Singleton, J.; McDonald, R.; Plonczak, A.; Kang, J.; Lee, C.; Whangbo, M.-H.; Lancaster, T.; Steele, A. J.; Franke, I.; Wright, J. D.; Blundell, S. J.; Pratt, F. L.; deGeorge, J.; Turnbull, M. M.; Landee, C. P. *Inorg. Chem.* **2012**, *51*, 2121−2129.

(7) Sobota, P.; Utko, J.; Jerzykiewicz, L. B. *Inorg. Chem.* **1998**, *37*, 3428−3431.

(8) Duffy, W.; Venneman, J. E.; Strandburg, D. L.; Richards, P. M. *Phys. Rev. B* **1974**, *9*, 2220−2227.

(9) Lubben, M.; Meetsma, A.; Feringa, B. L. *Inorg. Chim. Acta* **1995**, *230*, 169−172.

(10) Chippindale, A. M.; Cowley, A. R.; Peacock, K. J. *Acta Crystallogr., Sect. C: Cryst. Struct. Commun.* **2000**, *C56*, 651−652.

(11) de Jongh, L. J.; Miedema, A. R. *Adv. Phys.* **1974**, *23*, 1.

(12) (a) Pawlak, P. L.; Panda, M.; Loloee, R.; Kucera, B. E.; Costes, J.-P.; Tuchagues, J.-P.; Chavez, F. A. *Dalton Trans.* **2011**, *40*, 2926−2931. (b) Nazarenko, L.; Pop, F.; Sun, Q.; Hauser, A.; Lloret, F.; Julve, M.; El-Ghayoury, A.; Avarvari, N. *Dalton Trans.* **2015**, *44*, 8855−8866.

(13) Takeda, K.; Mito, M.; Nakajima, K.; Kakurai, K.; Yamagata, K. *Phys. Rev. B: Condens. Matter Mater. Phys.* **2000**, *63*, 024425.

(14) Kou, H.-Z.; Gao, S.; Li, C. H.; Liao, D.-Z.; Zhou, B.-Z.; Wang, R.-J.; Li, Y. *Inorg. Chem.* **2002**, *41*, 4756−4762.

(15) Pinkowicz, D.; Podgajny, R.; Nitek, R.; Rams, M.; Majcher, A. M.; Nuida, T.; Ohkoshi, S.; Sieklucka, B. *Chem. Mater.* **2011**, *23*, 21−31.

(16) Data integration software: *SAINT, version 5.00*; Bruker AXS, Inc.: Madison, WI, 1999.

(17) Absorption correction software: *SADABS*; Bruker AXS, Inc.: Madison, WI, 1999.

(18) Structure solution and refinement software: *SHELXTL, version 5.0*; Bruker AXS, Inc.: Madison, WI, 1996.

(19) See, for example: (a) Goddard, P. A.; Singleton, J.; Sengupta, P.; McDonald, R. D.; Lancaster, T.; Blundell, S. J.; Pratt, F. L.; Cox, S.; Harrison, N.; Manson, J. L.; Southerland, H. I.; Schlueter, J. A. *New J. Phys.* **2008**, *10*, 083025. (b) Manson, J. L.; Lapidus, S.; Stephens, P. W.; Peterson, P. K.; Southerland, H. I.; Lancaster, T.; Blundell, S. J.; Steele, A. J.; Singleton, J.; McDonald, R. D.; Kohama, Y.; Del Sesto, R. E.; Smith, N. A.; Bendix, J.; Zvyagin, S. A.; Zapf, V.; Goddard, P. A.; Kang, J.; Lee, C.; Whangbo, M.-H. *Inorg. Chem.* **2011**, *50*, 5990−6009. (c) Manson, J. L.; Baldwin, A. G.; Scott, B. L.; Bendix, J.; del Sesto, R. E.; Goddard, P. A.; Singleton, J.; Lancaster, T.; Moeller, J. S.; Blundell, S. J.; Tran, H. E.; Pratt, F. L.; Kang, J.; Lee, C.; Whangbo, M.-H. *Inorg. Chem.* **2012**, *51*, 7520−7528. (d) Goddard, P. A.; Manson, J. L.; Singleton, J.; Franke, I.; Lancaster, T.; Steele, A. J.; Blundell, S. J.; Baines, C.; Pratt, F. L.; McDonald, R. D.; Valenzuela, O. A.; Corbey, J. F.; Southerland, H. I.; Sengupta, P.; Schlueter, J. A. *Phys. Rev. Lett.* **2012**, *108*, 077208. (e) Ghannadzadeh, S.; Moeller, J. S.; Goddard, P. A.; Lancaster, T.; Xiao, F.; Blundell, S. J.; Maisuradze, A.; Khasanov, R.; Manson, J. L.; Tozer, S.; Graf, D.; Schlueter, J. A. *Phys. Rev. B: Condens. Matter Mater. Phys.* **2013**, *87*, 241102R. (f) Lancaster, T.; Goddard, P. A.; Blundell, S. J.; Foronda, F. R.; Ghannadzadeh, S.; Möller, J. S.; Baker, P. J.; Pratt, F. L.; Baines, C.; Huang, L.; Wosnitza, J.; McDonald, R. D.; Modic, K. A.; Singleton, J.; Topping, C. V.; Beale, T. A. W.; Xiao, F.; Schlueter, J. A.; Barton, A. M.; Cabrera, R. D.; Carreiro, K. E.; Tran, H. E.; Manson, J. L. *Phys. Rev. Lett.* **2014**, *112*, 207201.

(20) Larson, A. C.; Von Dreele, R. B. *GSAS: General Structure Analysis System*; Los Alamos National Laboratory Report No. LAUR-86-748; Los Alamos National Laboratory: Los Alamos, NM, 1990.

(21) Wu, J.-Z.; Tanase, S.; Bouwman, E.; Reedijk, J.; Mills, A. M.; Spek, A. L. *Inorg. Chim. Acta* **2003**, *351*, 278−282.

(22) Adams, C. J.; Kurawa, M. A.; Orpen, A. G. *Inorg. Chem.* **2010**, *49*, 10475−10485.

DOI: 10.1021/acs.inorgchem.5b02162
Inorg. Chem. XXXX, XXX, XXX−XXX

(23) Sobota, P.; Utko; Szafert, S.; Janas, Z.; Glowiak, T. *J. Chem. Soc., Dalton Trans.* **1996**, 3469−3473.
(24) Ashcroft, N. W.; Mermin, N. D. *Solid State Physics*; Saunders College Publishing: Philadelphia, 1976.
(25) Fisher, M. E. *Am. J. Phys.* **1964**, *32*, 343−346.
(26) Ginsberg, A. P.; Lines, M. E. *Inorg. Chem.* **1972**, *11*, 2289−2290.
(27) Lines, M. E. *J. Phys. Chem. Solids* **1970**, *31*, 101−116.
(28) Abragam, A.; Bleaney, B. *Electron Paramagnetic Resonance of Transition Ions*; Oxford University Press: Oxford, 1970.
(29) Duboc, C.; Phoeung, T.; Zein, S.; Pecaut, J.; Collomb, M.-N.; Neese, F. *Inorg. Chem.* **2007**, *46*, 4905−4916.
(30) Pato-Doldan, B.; Singleton, J.; Zapf, V. Manuscript in preparation.
(31) Topping, C.; Manson, J. L.; Goddard, P. A.; Singleton, J.; Lancaster, T.; Blundell, S. J. Manuscript in preparation.
(32) Lancaster, T. Manuscript in preparation.
(33) Lynn, J. W.; Shirane, G.; Blume, M. *Phys. Rev. Lett.* **1976**, *37*, 154−157.
(34) Lovesey, S. W. *Theory of Neutron Scattering from Condensed Matter*; Clarendon Press: Oxford, U.K., Vol. *2*, 1987.
(35) Stone, M. B.; Lumsden, M. D.; Nagler, S. E.; Singh, D. J.; He, J.; Sales, B. C.; Mandrus, D. *Phys. Rev. Lett.* **2012**, *108*, 167202.
(36) Stone, M. B.; Ehlers, G.; Granroth, G. *Phys. Rev. B: Condens. Matter Mater. Phys.* **2013**, *88*, 104413.
(37) Zhang, W.; Jeitler, J. R.; Turnbull, M. M.; Landee, C. P.; Wei, M.; Willett, R. D. *Inorg. Chim. Acta* **1997**, *256*, 183−198.
(38) Unni Nair, B. C.; Sheats, J. E.; Ponteciello, R.; Van Engen, D.; Petrouleas, V.; Dismukes, G. C. *Inorg. Chem.* **1989**, *28*, 1582−1587.

DOI: 10.1021/acs.inorgchem.5b02162
Inorg. Chem. XXXX, XXX, XXX−XXX